A refraction-corrected tomographic algorithm for immersion laser-ultrasonic imaging of solids with piecewise linear surface profile

V. Zarubin,[1,2,a)] A. Bychkov,[1,2] V. Simonova,[3] V. Zhigarkov,[4] A. Karabutov,[1,3,5] and E. Cherepetskaya[1]

[1)] *The National University of Science and Technology MISIS, 6 Leninsky prospekt, 119049 Moscow, Russia*

[2)] *Faculty of Physics, Lomonosov Moscow State University, 1 Leninskie Gory, 119991 Moscow, Russia*

[3)] *The Institute on Laser and Information Technologies of the Russian Academy of Sciences, 1 Svyatoozerskaya St., 140700 Shatura, Moscow Region, Russia*

[4)] *The Institute of Photonic Technology, FRSC "Crystallography and Photonics" of the Russian Academy of Sciences, 2 Pionerskaya St., 108840 Troitsk, Moscow, Russia*

[5)] *International Laser Center, Lomonosov Moscow State University, 1 Leninskie Gory, 119991 Moscow, Russia*

(Dated: 15 May 2018)

In this paper a technique for reflection mode immersion 2D laser-ultrasound tomography of solid objects with piecewise linear 2D surface profiles is presented. Pulsed laser radiation was used for generation of short ultrasonic probe pulse providing high spatial resolution. Piezofilm sensor array was used for detection of the waves reflected by surface and internal inhomogeneities of the object. The original ultrasonic image reconstruction algorithm accounting for refraction of acoustic waves at the liquid-solid interface provided longitudinal resolution better than 100 μm in PMMA sample object.

Keywords: laser ultrasound, solids, tomographic imaging, algorithms, refraction.

While non-destructive testing and evaluation of objects with complex shapes have numerous practical applications, it poses a significant challenge. X-ray computed tomography, used often to solve this task, requires access to the object from all sides and has low spatial resolution for visualization of small internal cracks. These features limit the applicability of x-ray tomography and can be partially overcome by ultrasonic methods. Laser ultrasonic structuroscopy with a single transducer[1,2] is one of the well-established methods providing high spatial resolution (better than 100 μm) in various materials, absense of "dead zone" and side-lobes typical for conventional ultrasonic transducers and capable of speed of sound measurements with high precision exceeding 0.5%. The advantages of this method originate from the smooth aperiodic waveform and short duration of the laser-generated ultrasonic pulse, as pulsed laser radiation can be used to generate picosecond[3] and even femtosecond[4] acoustic pulses for diagnostics of thin layered structures, as well as arbitrary ultrasonic fields[5].

Elaborate positioning systems with 4 or 5 degrees of freedom are developed to inspect objects with complex shapes with a single transducer. Such systems move the transducer along the surface of the object in a raster-scanning fashion. However, this approach has relatively low performance, insufficient for some applications. The tomographic approach uses an array of transducers to increase the performance and improve image quality. Today ultrasonic tomographic systems for inspection of flat-surfaced solid parts are widely used[6,7]. Parts with smooth non-planar surface can be inspected with flexible phased arrays[8,9].

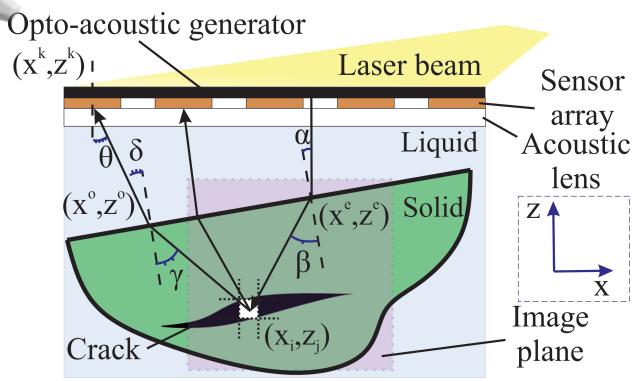

FIG. 1. Principle of the immersion laser ultrasonic imaging and schematic of the proposed algorithm. Paths of the longitudinal BAWs: forward – on the right-hand side of the figure, backward – on the left-hand side.

The goal of the current research is the application of the optoacoustic effect to the yet unsolved problem of ultrasonic imaging of solid bodies and investigation of the effects and artifacts that influence image quality. We propose an experimental system and technique for immersion laser ultrasonic tomographic imaging of samples with piecewise linear surface profiles. The problem of tomography of solids is complicated, and this task required developing a novel laser ultrasonic image reconstruction algorithm accounting for refraction. The principle of the technique is presented in Fig 1. The light-absorbing plate (opto-acoustic generator) under the impact of a nanosecond laser pulse gets locally heated, and that leads to the thermoelastic expansion and generation of an ultrasonic

[a)] Electronic mail: zarubin.vasily@gmail.com

probe pulse with a plane wavefront. This wave is focused by an acoustic lens to form the image plane of approximately 0.5 mm thickness[10]. The piezoelectric sensor array records acoustic waves reflected from internal cracks and other acoustic inhomogeneities of the object. The recorded waveforms are processed to reconstruct a 2D image of a part of the object – a laser-ultrasonic tomogram. The aforementioned acoustic lens improves the spatial resolution of the setup in the direction perpendicular to the image plane.

The proposed technique allows real-time inspecting of solid parts with high spatial resolution due to combined advantages of laser generation of ultrasound, array signal detection and tomographic image reconstruction. In this paper, we assume that the 2D surface profile of the object can be represented as a piecewise linear curve which is relevant for a wide class of industrial tasks (e.g. composite pipes with varying diameter). While the proposed algorithm can be applied with other ways of ultrasound generation, the use of optoacoustic mechanism for profilometry and imaging can be advantageous. The reflected aperiodic laser ultrasonic probe pulse is recorded by the wideband piezofilm sensor array. Short duration (typically less than 100 ns) of the probe pulse enables high spatial resolution. Many conventional ultrasound systems have the "dead zone" – the region right under the surface of the sample where the signals from the internal structure of the sample overlap with the ringing caused by the pulse reflected from the surface. Highly damped piezoelectric transducers provide wider bandwidth and smaller "dead zone" but smaller penetration depth. The use of optoacoustic mechanism decouples generation and reception of ultrasound and leads to the mitigation of the "dead zone"' if highly damped transducer is used. Also the transverse pressure profile of the laser ultrasonic probe pulse corresponds to the transverse profile of the laser pulse and has no sidelobes.

Ultrasonic image reconstruction of the interior of a solid object is an ill-posed problem due to incompleteness of data acquired from a limited viewing angle, inherent sensitivity of ultrasonic measurements to surface roughness, weak inhomogeneities of density, speed of sound, state of matter and crystal structure and other parameters, which can vary over the sample volume. We assume that sample and immersion liquid are two homogenious media that have piecewise linear interface. The proposed algorithm is based on the heuristic ray-tracing technique and has three stages: 1) reconstruction of a 2D laser ultrasonic tomogram using standard filtered back-projection algorithm for homogeneous media; 2) segmentation of sample 2D surface profile from the tomogram; 3) refraction-corrected re-reconstruction of the part of the tomogram related to interior of the sample object.

First, the filtered back-projection algorithm[11] reconstructs the 2D laser ultrasonic image over the parabolic "arcs of probability". Let the acoustic inhomogeneity be located at the point $\boldsymbol{r} = (x, z)$ of the tomogram and the plane opto-acoustic generator – at $z = z_g$. The generated plane ultrasonic wave travels the distance of $z - z_g$ along z-axis through the immersion liquid to the point $\boldsymbol{r}$, where it is partially scattered or reflected backwards, and then it is detected by the m-th transducer at the point $\boldsymbol{d}_m = (x_m, z_m)$. Hence, the total travel time is $t_m = (z - z_g + |\boldsymbol{d}_m - \boldsymbol{r}|)/c_0$, where c_0 is the speed of sound in the immersion liquid. The amplitude of the wave detected at $\boldsymbol{d}_m$ is proportional to the strength of the scatterer or the reflection coefficient of the boundary located at $\boldsymbol{r}$. In the first Born approximation or single reflection approximations the elemental scatterer or the reflecting boundary do not change the waveform of the incident pulse changing only its amplitude with the directivity pattern that depends on the type of the inhomogeneity. Thus, the strength of the scatterer or the reflection coefficient of the boundary at $\boldsymbol{r}$ can be found by taking the amplitude of the pressure signal detected at $\boldsymbol{d}_m$ at time t_m and compensating for the directivity of the scatterer, directivity of the receiver and $1/r$ attenuation of spherical waves. Assuming the scatterers are monopole and scatter the incident waves omnidirectionally, the effective amplitude of acoustic inhomogeneity represented by back-projected acoustic pressure:

$$\epsilon(\boldsymbol{r}) = \sum_{m=1}^{N} p\left(\boldsymbol{d}_m, t_m\right) \cdot |\boldsymbol{d}_m - \boldsymbol{r}| \cdot D(\boldsymbol{d}_m, \boldsymbol{r}), \qquad (1)$$

where $p(\boldsymbol{d}_m, t)$ is the acoustic pressure signal recorded by the m_{th} transducer, $D(\boldsymbol{d}_m, \boldsymbol{r})$ is the directivity pattern of the m-th transducer. The function $D(\boldsymbol{d}_m, \boldsymbol{r})$ is introduced here to reduce strong arc-like image artifacts that appear when the sensor array has a relatively small number of receivers N. We approximate the directivity pattern with that of a rectangular transducer:

$$D(\boldsymbol{d}_m, \boldsymbol{r}) = \cos\left(\frac{\pi}{2}\frac{\theta}{\Theta}\right), \ \theta = \operatorname{atan}\left(\frac{z - z_g}{|\boldsymbol{d}_m - \boldsymbol{r}|}\right), \qquad (2)$$

which depends on the angle θ between the normal vector to the transducer surface coinciding with the z-axis direction and vector $(\boldsymbol{r} - \boldsymbol{d}_m)$ from the transducer center to the image point, and $\Theta \approx 0.3$ is defined by the transducer parameters.

The second step is to segment a profile in the reconstructed tomogram[12]. The acoustic impedance of the solid with respect to longitudinal bulk acoustic waves (BAW) is $Z_1^n = \rho_1 c_1$, where ρ_1 is the density of sample and c_1 is the speed of longitudinal BAW. The acoustic impedance of solids is usually greater than the acoustic impedance of the immersion liquid $Z_0^n = \rho_0 c_0$, where ρ_0 is the immersion liquid density. Pressure reflection coefficient for the normal wave incidence to the sample surface is $R^n = (Z_1^n - Z_0^n)/(Z_1^n + Z_0^n)$. Hence, the probing ultrasonic pulse retains the sign upon reflection, and the first maximum of the reconstructed tomogram corresponds to the surface of the sample. We denote a set of points (x, z) where the laser ultrasonic image has a local maximum along the z-axis as

This manuscript was accepted by Appl. Phys. Lett. Click here to see the version of record.

$$M = \left\{ (x,z) : \left.\frac{\partial \epsilon}{\partial z}\right|_{(x,z)} = 0, \left.\frac{\partial^2 \epsilon}{\partial z^2}\right|_{(x,z)} < 0 \right\}. \quad (3)$$

The reconstructed profile $p(x)$ is a subset of M where the points have the maximum z-coordinate for each x-coordinate. In this paper solid objects with piesewise linear surface profiles are considered. To identify all linear segments in the set $p(x)$ we used the Hough transform[13] of the laser ultrasonic image. The Hough transform is related to the Radon transform and as a result it produces a matrix A, each element $A(\tilde{\rho}, \tilde{\varphi})$ is proportional to the probability that the line with polar coordinates $(\tilde{\rho}, \tilde{\varphi})$ exists in the profile $p(x)$. The elements with locally maximum probabilities form a set of approximate line positions, and then the equations $z = k_s x + b_s$ can be obtained by applying the least squares method to the profile $p(x)$.

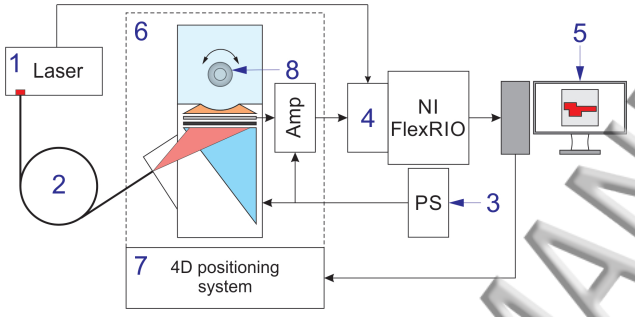

FIG. 2. Experimetnal setup[12]. 1 — Nd:YAG laser, 2 — optical fiber, 3 — power supply, 4 — data acquisition and processing system, 5 — personal computer with GPU, 6 — wideband laser-ultrasonic module (opto-acoustic generator, acoustical lens, antenna of sensors and multichannel preamplifier), 7 — 4-axis positioning system, 8 — sample.

The third step is to re-reconstruct the part of the laser ultrasonic image under the profile obtained at the second step. Pixels with coordinates $\{(x_i, z_j) : z_j < k_s x_i + b_s\}$ represent the interior of sample object. To calculate the correct travel time taking into account refraction at the liquid-solid interface, the overall path is divided into forward and backward parts (Fig. 1). The total travel time from the generator to the acoustic inhomogeneity at point $\boldsymbol{r}_{ij} = (x_i, z_j)$ inside the sample object (denote t_{ijm}^{forw}) and back (denote t_{ijm}^{back}) to the m-th transducer is $t_{ijm} = t_{ijm}^{\text{forw}} + t_{ijm}^{\text{back}}$.

On the forward path, the angle of incidence α and the angle of refraction β are related by the Snell's law:

$$\sin\alpha / c_0 = \sin\beta / c_1, \quad (4)$$

where c_1 is speed of sound in the sample object, and $\alpha = \text{atan}(k_s^\nu)$ is defined by the ν-th piecewise linear part of sample surface crossed by the corresponding acoustic ray. From 4 the coordinates of the refraction point of the forward-going acoustic ray (x_{ijm}^e, z_{ijm}^e) can be calculated. Hence, forward travel time is calculated as

$$t_{ijm}^{\text{forw}} = \frac{z_{ijm}^e - z_g}{c_0} + \frac{1}{c_1}\sqrt{(x_{ijm}^e - x_i)^2 + (z_{ijm}^e - z_j)^2}. \quad (5)$$

On the backward path, as it follows from the Fermat's principle of least time, the travel time from the inhomogeneity at (x_i, z_j) to the m-th transducer

$$t_{ijm}^{\text{back}}(x^o, z^o) = \frac{\sqrt{(x_m - x^o)^2 + (z_m - z^o)^2}}{c_0} + \frac{\sqrt{(x_i - x^o)^2 + (z_j - z^o)^2}}{c_1}, \quad (6)$$

has to be minimal. Here (x_{ijm}^o, z_{ijm}^o) are the coordinates of the refraction point of the backward-going acoustic ray on the solid-liquid interface that can be obtained from the system of equations:

$$\begin{cases} (x_{ijm}^o, z_{ijm}^o) = \underset{(x^o, z^o)}{\text{argmin}}\, t_{ijm}^{\text{back}}(x^o, z^o), \\ z^o = k_s x^o + b_s. \end{cases} \quad (7)$$

In the case of the more complicated surface profile than piecewise linear, the second equation in 7 has to be changed accordingly. To solve this system and calculate x_{ijm}^o we used the iterative gradient descent:

$$x_{n+1}^o = x_n^o - \lambda_n \frac{\partial t_{ijk}^{\text{back}}}{\partial x^o}, \quad (8)$$

where step λ_n decreased with each iteration. The iterative process was terminated when $|x_{n+1}^o - x_n^o| \lesssim 5$ μm.

Careful calculation of tomogram pixels inside the sample requires corrections for the transmission coefficients of longitudinal BAW through the liquid-solid interface at the points of refraction on the forward path – W^{el}, and on the backward path – W^{ol}, given by[14]

$$W^{el} = \frac{\rho_0}{\rho_1} \frac{2 Z_l \cos 2\beta_1}{Z_l \cos^2 2\beta_1 + Z_t \sin^2 2\beta_1 + Z}, \quad (9)$$

$$W^{ol} = \frac{c_0 \cos\gamma}{c_1 \cos\delta \cos^2 2\beta_2} \cdot \frac{2 Z_l^o \cos^2 2\gamma}{Z^o + Z_t^o \sin^2 2\gamma + Z_l^o \cos^2 2\gamma}. \quad (10)$$

Here α and γ are the angles of incidence, β and δ are the angles of refraction of probing and scattered longitudinal BAWs correspondingly, β_1 – angle of refraction of the shear BAW generated at (x_{ijk}^e, z_{ijk}^e), β_2 is the angle of reflection of the shear BAW generated at (x_{ijk}^o, z_{ijk}^o), $Z = \rho_0 c_0 / \cos\alpha$, $Z_l = \rho_1 c_1 / \cos\beta$, $Z_t = \rho_1 b_1 / \cos\beta_1$, $Z^o = \rho_0 c_0 / \cos\delta$, $Z_l^o = \rho_1 c_1 / \cos\gamma$, $Z_t^o = \rho_1 b_1 / \cos\beta_2$, b_1 is the speed of shear BAW in the sample.

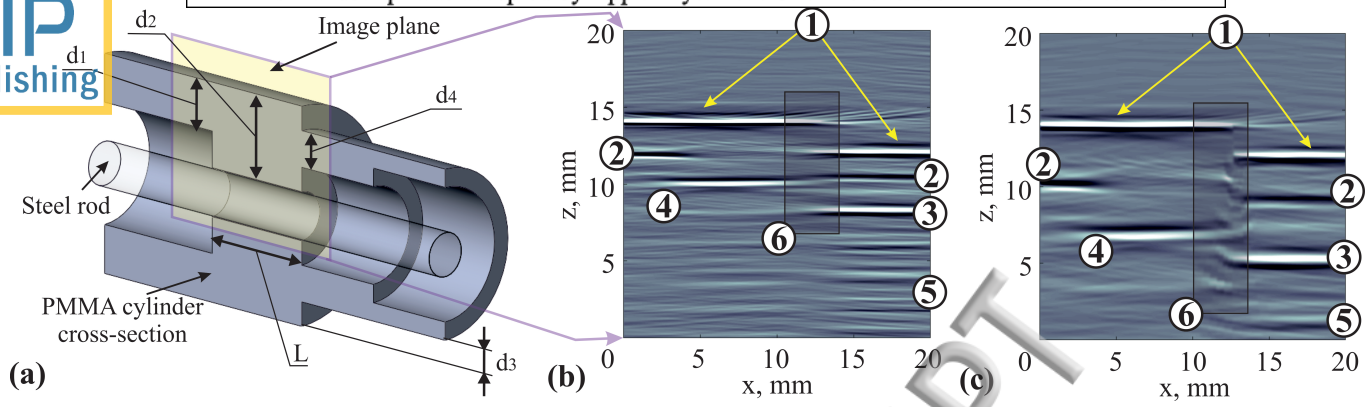

FIG. 3. (a) The cross-sectioned 3D model of the sample object: PMMA solid of revolution with complex external and internal generatrices fixed on a steel rod and submerged in water. (b) The reconstructed laser ultrasonic image of the sample object after the first stage of the algorithm (without refraction correction). (c) The final refraction-corrected image. Black and white stripes show the position of the boundaries that reflect the ultrasonic probe pulse and the sign of the acoustic reflection coefficient (black – negative, white – positive). The sensor array is located at $z \approx 50.1$ mm. 1, 2 – external and internal surfaces of the sample, reflection on the solid-water interface, 3 – reflection from the steel rod, 4 – internal surfaces of the sample, reflection on the steel-PMMA interface with a gap of water, 5 – reverberations, 6 – area with image artifacts.

Therefore, 1 can be modified to re-reconstruct the image of the interior of the sample in the following way:

$$\epsilon'(\boldsymbol{r}_{ij}) = \sum_{m=1}^{N} p\left(\boldsymbol{d}_m, t_{ijk}\right) \cdot D(\boldsymbol{d}_m, \boldsymbol{r}_{ij}) \cdot W_{ijk}^{ol} W_{ijk}^{el}. \quad (11)$$

We used the universal system for combined real-time opto-acoustic and laser-ultrasonic imaging[15] in laser ultrasonic mode to verify experimentally the proposed algorithm (Fig. 2). Following the principle discussed above, it uses pulsed laser radiation of a Q-switched Nd:YAG laser with wavelength $\lambda = 1064$ nm, pulse duration $\tau = 10$ ns, pulse repetition rate of 20 Hz for excitation of ultrasound wave in the opto-acoustic generator. The excited laser ultrasonic bipolar pulse has a duration of 150 ns (full-width at half-maximum) and its bandwith is 0.1 –15 MHz. The movement of the sample object is performed by the positioning system with 4 degrees of freedom including a rotational axis (0.2° precision) and three translational axes (10 μm precision). The probe acoustic pulse is focused onto the sample, reflected from the surface and internal inhomogeneities and then recorded by the cylindrical array of 16 polyvinylidene fluoride piezofilm transducers with effective reception band of 1.6—9 MHz[16].

Dimensions	d_1	d_2	d_3	d_4	L
LU, mm	3.84	6.95	1.96	2.90	9.80
Gauge, mm	3.92	7.05	1.99	2.97	10.07

TABLE I. Comparison of measurements by means of laser ultrasonic (LU) imaging and standard gauge.

The FPGA-based high-speed acquisition system with analog-to-digital converter (12 bit, 50 MS/s, 32 channels, NI 5752) pre-amplified, digitized, averaged over multiple laser shots and transferred the analog signals from the array of piezoelectric transducers to the PC for Fourier filtering and image reconstruction using the algorithm described earlier. The first step of the algorithm was implemented using NVIDIA CUDA parallel computing technique on the graphical card GeForce 770 GTX in real time. Real-time coarse imaging mode allowed to position the sample object in the focal plane properly to get the sharpest image for further processing. The subsequent steps were performed in MATLAB afterwards.

A PMMA body of revolution was manufactured (Fig. 3, (a)) for algorithm testing. The selected sample shape simulates an industrial part and allows clear demonstration of image reconstruction. The image of the part of the sample reconstructed by the back-projection algorithm with and without refraction correction steps are compared in Fig. 3, (b) and (c), respectively. Without refraction correction the sample appears "squeezed" in the z-axis direction since the speed of longitudinal BAWs in PMMA is 1.8 times greater than in water. The proposed refraction-corrected algorithm reveals the actual dimensions of the sample. The reflection coefficients of the external (liquid-solid) and internal (solid-liquid) boundaries have the opposite signs due to the PMMA having greater acoustic impedance than water. That is why the external boundary (1) is white and the internal boundary (2) is black. The sample has a cylindrical hole for a holder (small steel rod). Steel has the highest acoustic impedance in the setup, so the PMMA-steel and water-steel boundaries are white (3 and 4). Reflection (4) is formed on the PMMA-steel interface with a thin water gap. The pulse reflected from the steel rod travels back and forth in the water layer between the rod and the internal surface of the sample object generating multiple reverberations (5). The area delineated by the black rectangle (6) contains image artefacts caused by the limited number of sensors and their finite size. Re-

flections (3) and (4) in Fig. 3, (c) come from the surface of the steel rod, but they do not form a straight line. The proposed algorithm assumes that after the refraction at the piecewise linear external surface of the sample object the BAWs propagate only in the solid sample and do not undergo subsequent refractions. However, in the region $x > 13$ mm (Fig. 3) BAWs pass through the external boundary (1) and through the internal boundary (2) of the solid object. Then BAWs pass through a water layer between (2) and (3), reflect from the steel rod and travel back. The algorithm assumes that the water layer is the solid sample and does not reconstruct the distance between (2) and (3) correctly.

The sample dimensions (Fig. 3, (b)) were measured by the laser ultrasonic method and by the standard gauge to check the accuracy of the algorithm. The results of this comparison are presented in Tab. I. The longitudinal (along z-axis) accuracy is significantly better than 100 μm, but the transverse (along x-axis) error is 200-300 μm. The accuracy of longitudinal measurements is mainly determined by the accuracy of the speed of longitudinal BAW measurements. The relatively low transverse resolution is typical for most ultrasonic methods and limits the scope of the proposed technique.

One of the important sources of error was the acoustic lens made of PMMA. In the image plane it was $h = 3$ mm thick. Both the probe pulse and the reflected pulses undergo refraction at the water-PMMA boundary. Since the lens is relatively thin, this refraction can be partially mitigated by replacing the PMMA lens with water layer $\Delta z_g = 2h(1 - c_0/c_1) \approx 2.63$ mm thick. In this case the error in the direction perpendicular to the lens boundary is completely compensated. The error for oblique incidence estimated from geometrical acoustics (for angles of incidence less than $\Theta_{max} = 0.3$) is less than 36 μm. This error slightly broadens the recorded reflected pulse and the black and white stripes in Fig. 3, (b), (c).

In the present study the width of ultrasonic probe pulse beam along x-axis exceeded 20 mm, and the maximum angle between the sample surface and the sensor array did not exceed 10°. In this case the transmission of energy from longitudinal BAWs in water to shear BAWs in the sample can be neglected. That is why the "LL" imaging mode was used. In this mode the longitudinal BAWs in water are converted to longitudinal BAWs in the sample during refraction at the external surface (the first 'L' in "LL"). Then the scatterer converts longitudinal BAWs in the sample to the longitudinal BAWs in the sample (the second 'L') and these scattered BAWs are converted to the longitudinal BAWs in water. However, if the amplitude of shear BAWs is significant, "SL" or "SS" imaging modes can be used. In these cases, the speed of BAWs in the sample c_1 and transmission coefficients W^{el} and W^{ol} in the formulas above should be changed accordingly.

In conclusion, we proposed the algorithm for immersion 2D laser ultrasonic tomography of solid objects with complex surface profile, which is based on the ray-tracing method and accounts for the refraction of laser ultrasonic beam on solid-liquid interface on the forward and backward paths. The algorithm can be parallelized on a single PC for real-time high-speed measurements of internal geometry of samples on the production line. If one provides a sample model, which can be a set of linear equations, then the deviation of the sample real shape from the model shape can be calculated. The algorithm was tested on the experimental data obtained from the PMMA solid of revolution by the broadband real-time laser ultrasonic imaging system. The experimental results are in good agreement with the standard gauge measurements.

This work is supported by NUST MISIS Competitiveness Program by the Ministry of Education and Science of the Russian Federation (№ K2-2017-003), by Russian Science Foundation (16-17-10181) in part of the setup and algorithms development and by the Federal Agency of Scientific Organizations (Agreement № 007-GZ/Ch3363/26) in part of algorithms implementation.

[1] A. Karabutov, A. Devichensky, A. Ivochkin, M. Lyamshev, I. Pelivanov, U. Rohatgi, V. Solomatin, and M. Subudhi. Laser ultrasonic diagnostics of residual stress. *Ultrason.*, 48(6-7), 2008.

[2] I. Pelivanov, A. Shtokolov, C.W. Wei, and M. O'Donnell. A 1-kHz A-Scan Rate Pump-Probe Laser-Ultrasound System for Robust Inspection of Composites. *IEEE Trans. Ultrason., Ferroelect., Freq. Control*, 62(9), 2015.

[3] J. Faria, P. Garnier, and A. Devos. Non-destructive spatial characterization of buried interfaces in multilayer stacks via two color picosecond acoustics. *Appl. Phys. Lett.*, 111(24), 2017.

[4] H.Y. Chen, Y.R. Huang, H.Y. Shih, M.J. Chen, J.K. Sheu, and C.K. Sun. Extracting elastic properties of an atomically thin interfacial layer by time-domain analysis of femtosecond acoustics. *Appl. Phys. Lett.*, 111(21), 2017.

[5] M.D. Brown, D.I. Nikitichev, B.E. Treeby, and B.T. Cox. Generating arbitrary ultrasound fields with tailored optoacoustic surface profiles. *Appl. Phys. Lett.*, 110(9), 2017.

[6] L.C. Lynnworth. *Ultrasonic measurements for process control: theory, techniques, applications*. Academic Press, 2013.

[7] *Advances in Phased Array Ultrasonic Technology Applications*. Olympus NDT, 2007.

[8] K. Nakahata, S. Tokumasu, A. Sakai, Y. Iwata, K. Ohira, and Y. Ogura. Ultrasonic imaging using signal post-processing for a flexible array transducer. *NDT E Int.*, 82, 2016.

[9] O. Casula, G. Toullelan, O. Roy, and P. Dumas. Ultrasonic nondestructive testing of complex components with flexible phased-array transducers. *ECNDT Proceedings, 10th European Conference on Non-Destructive Testing*, 2010.

[10] T.D. Khohlova, I.M. Pelivanov, and A.A. Karabutov. Optoacoustic tomography utilizing focused transducers: The resolution study. *Appl. Phys. Lett.*, 92(2), 2008.

[11] G. Wurzinger, R. Nuster, N. Schmitner, S. Gratt, D. Meyer, and G. Paltauf. Simultaneous three-dimensional photoacoustic and laser ultrasound tomography. *Biomed. Opt. Express*, 4(8), 2013.

[12] V. Zarubin, A. Bychkov, A. Karabutov, V. Simonova, and E. Cherepetskaya. Laser-induced ultrasonic imaging for measurements of solid surfaces in optically opaque liquids. *Appl. Opt.*, 57(10), 2018.

[13] R. Szeliski. *Computer Vision: algorithms and applications*. Springer Science and Business Media, 2010.

[14] L. Brekhovskih. *Waves in Layered Media*. Academic Press, 1976.

[15] A. S. Bychkov, V. P. Zarubin, A. A. Karabutov, V. A. Simonova, and E. B. Cherepetskaya. On the use of an optoacoustic and laser ultrasonic imaging system for peripheral intravenous access. *Photoacoustics*, 5, 2017.

[16] V.A. Simonova, T.D. Khohlova, and A.A. Karabutov. Wideband focused transducer array for optoacoustic tomography. *Acoust. Phys.*, 55(6), 2009.